Optical properties of gold films and the Casimir force

V. B. Svetovoy[*]

MESA + Research Institute, University of Twente, PO 217, 7500 AE Enschede, The Netherlands

P. J. van Zwol, G. Palasantzas, and J. Th. M. De Hosson

Department of Applied Physics, Netherlands Institute for Metals Research and Zernike Institute for Advanced Materials, University of Groningen, Nijenborgh 4, 9747 AG Groningen, The Netherlands

Precise optical properties of metals are very important for accurate prediction of the Casimir force acting between two metallic plates. Therefore we measured ellipsometrically the optical responses of Au films in a wide range of wavelengths from 0.14 to 33 μm. The films at various thicknesses were deposited at different conditions on silicon or mica substrates. Considerable variation of the frequency dependent dielectric function from sample to sample was found. Detailed analysis of the dielectric functions was performed to check the Kramers-Kronig consistency, and extract the Drude parameters of the films. It was found that the plasma frequency varies in the range from 6.8 to 8.4 eV. It is suggested that this variation is related with the film density. X-ray reflectivity measurements support qualitatively this conclusion. The Casimir force is evaluated for the dielectric functions corresponding to our samples, and for that typically used in the precise prediction of the force. The force for our films was found to be 5%–14% smaller at a distance of 100 nm between the plates. Noise in the optical data is responsible for the force variation within 1%. It is concluded that prediction of the Casimir force between metals with a precision better than 10% must be based on the material optical response measured from visible to mid-infrared range.

I. INTRODUCTION

The force between electrically neutral metallic plates separated by a small vacuum gap (of micron and/or submicron dimensions), as predicted by the eminent Dutch physicist Casimir in 1948, still attracts considerable interest. On one hand this interest is curiosity driven since the force is connected with the zero-point fluctuations in vacuum, and on the other hand the interest stems from practical applications because modern microtechnology approaches the limit where the force starts to influence the performance of microdevices. During the past decade the Casimir force was measured with increasing precision in a number of experiments using different techniques such as torsion pendulum,[2] atomic force microscope (AFM),[3,4] microelectromechanical systems,[5–8] and different geometrical configurations: sphere-plate,[2,4,7] plate-plate,[9] and crossed cylinders.[10] In most cases the bodies were covered with gold evaporated or sputter deposited to a thickness of 100–200 nm.

Relatively low precision, 15%, in the force measurement was reached for the plate-plate configuration[9] because of the parallelism problem. In the torsion pendulum experiment[2] the force was measured with an accuracy of 5%. In the experiments[4,5,10] errors were claimed on the level of 1%. In the most precise up to date experiment[6–8] the experimental errors claimed to be as low as 0.5%.

Comparison between theory and experiment answers an important question: How accurately do we understand the origin of the force? To make a precise evaluation of the force taking into account real conditions of the experiments is equally difficult as to make a precise measurement. In its original form, the Casimir force[1] given by

$$F_c(a) = -\frac{\pi^2}{240}\frac{\hbar c}{a^4} \tag{1}$$

was calculated between the ideal metals at zero temperature. It depends only on the fundamental constants and the distance between the plates a. The force between real materials was derived for the first time by Lifshitz and co-workers.[11–13] The material properties enter the Lifshitz formula via the frequency dependent dielectric function $\varepsilon(\omega)$. This formula became the basis for all precise calculations of the force. Corrections to Eq. (1) can be very large especially at small separations (<100 nm) between bodies. The Lifshitz formula accounts for real optical properties of the materials, and for finite temperature effects. An additional source of corrections to the force is the surface roughness of interacting plates.[14–16]

In all the experiments mentioned above the bodies were covered with metallic films but the optical properties of these films have never been measured. It is commonly accepted[4,7,8,17] that these properties can be taken from the handbooks' tabulated data[18,19] together with the Drude parameters, which are necessary to extrapolate the data to low frequencies. This might still be a possible way to estimate the force, but it is unacceptable for calculations with controlled precision. Lamoreaux[20] was the first who recognized this problem. The reason is very simple:[20–23] optical properties of deposited films depend on the method of preparation, and can differ substantially from sample to sample.

Recently analysis of existing optical data for Au was undertaken[24] to explore how significant is the effect of variation of the optical properties on the Casimir force. It was demonstrated that different sets of the data deviate considerably. This variation influences the Casimir force on the level
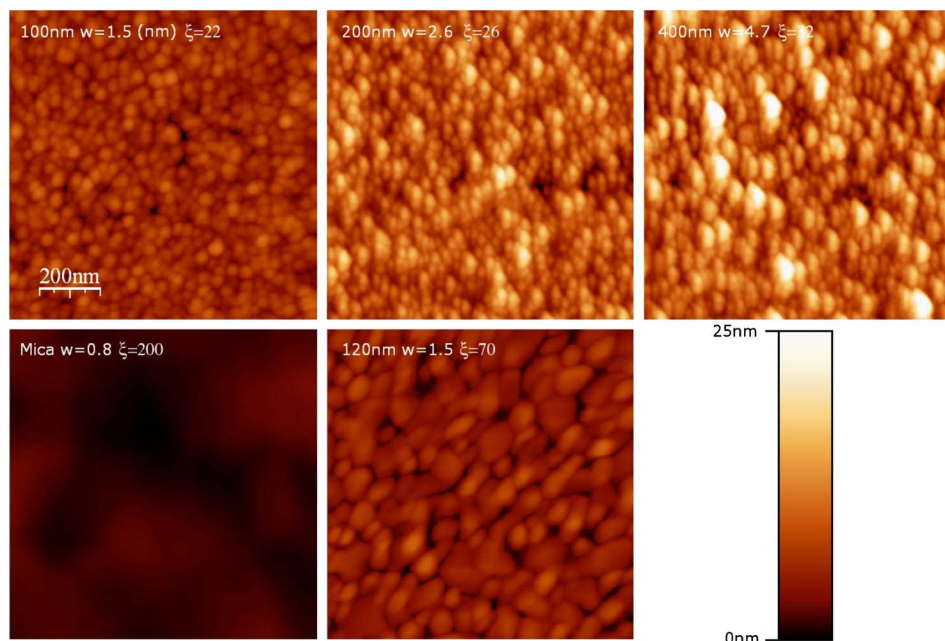
FIG. 1. (Color online) Surface scans of all films with AFM using the same color scale. The scan area is 1 μm^2. The film thickness, rms roughness w, and correlation length ξ are shown in each panel (in nm).

of 5% in the distance range of the most precise experiments. Significant sample dependence of the force raises doubts on reported agreement between theory and experiment within 1% precision.[4,8] This is an important issue that has to be further thoroughly investigated.

In this paper we present the optical properties of Au films of different thicknesses deposited in two different evaporators on silicon and/or mica substrates, unannealed or annealed after the deposition. Moreover, we will discuss the influence of measured optical properties of gold films on the precise evaluation of the Casimir force. The characterization of the films was performed over a wide frequency range. It was done ellipsometrically using the infrared variable angle spectroscopic ellipsometer in the wavelength range 1.9–33 μm, and the vacuum ultraviolet ellipsometer in the range 0.14–1.7 μm. In addition, the film roughness was characterized with AFM, and the electron density in the films was estimated from x-ray reflectivity measurements.

Careful analysis of the data is performed to extract the values of the Drude parameters. It includes joint fits of the real and imaginary parts of the dielectric function, or refractive index and extinction coefficient in the low frequency range; the Kramers-Kronig consistency of the dielectric function or complex refractive index performed at all frequencies. The most important conclusions that follow from this analysis are that the films deposited at the same conditions, but having different thicknesses, have considerably different dielectric functions; annealing or change of the deposition method showed also influence on the optical properties. At any rate this difference cannot be ignored in a precise calculation of the Casimir force. We demonstrate that the optical data typically used for the force evaluation in former studies are far away from those found in our samples. The main reason for this deviation is the use of the Drude parameters, which correspond to a perfect gold single crystal rather than real polycrystalline films, containing a number of different defects.

The paper is organized as follows. In Sec. II we describe preparation and characterizations of Au films and make comparison with results known from literature. Analysis of the optical data is presented in Sec. III, where the Drude parameters, and uncertainties in these parameters are determined. Calculation of the Casimir force for our samples is given in Sec. IV. Our conclusions are presented in Sec. V.

II. EXPERIMENT

Five gold films were prepared by Au deposition on cleaned (100) Si substrates and freshly cleaved mica. The native oxide on Si substrates was not removed; the root-mean-square (rms) roughness was 0.3 nm for the Si substrates, while the mica substrate was atomically flat. The first three samples (numbered as 1, 2, and 3) were prepared on Si covered first with 10 nm adhesive sublayer of titanium followed by deposition of 400, 200, and 100 nm of Au from the source of 99.999% purity. The electron-beam evaporator was used for deposition at a base pressure of 10^{-6} mbar. The deposition rate was 0.6 nm/s. The temperature of the samples was not controlled in the evaporator and it was approximately at room temperature. The other two samples were prepared in a thermal evaporator at the same base pressure and deposition rate. One film was deposited to a thickness of 120 nm on Si with chromium sublayer (sample 4). The other film of the same thickness was deposited on mica, annealed at 375 °C (2 h), and slowly cooled down in a period of 6 h resulting in an atomically flat film (sample 5).

The atomic force microscope (Veeco Dimension 3100) was used to determine the surface morphology. The roughness scans are shown in Fig. 1 for all five samples. The corresponding rms roughness, w, and correlation length,[25–27] ξ, shown in each panel, were obtained as the average values found from multiple scans. The correlation lengths for the first three samples corresponding to the lateral feature sizes were reported before.[28] It should be noted that for sample 4

(120 nm Au/Si) the correlation length is larger than those for the other three films on Si. It can result from differences in the evaporation process or due to different adhesive layers. The annealed film on mica had very smooth hills and the largest correlation length.

Optical characterization of the films was performed by J. A. Woollam Co., Inc.[29] The vacuum ultraviolet variable angle spectroscopic ellipsometer (VASE) was used in the spectral range from 137 to 1698 nm at two angles of incidence 65° and 75° (±0.01°). The steps in the wavelength λ was increased quadratically with λ from 1.5 to 200 nm. In the spectral range from 1.9 to 32.8 μm the infrared variable angle spectroscopic ellipsometer (IR-VASE) was used at the same incidence angles in steps $\sim \lambda^2$ ranging from 1.4 to 411 nm.

From ellipsometry the ratio of p-polarized and s-polarized complex Fresnel reflection coefficients is obtained[30,31] as follows:

$$\rho = \frac{r_p}{r_s} = \tan \Psi e^{i\Delta}, \tag{2}$$

where $r_{p,s}$ are the corresponding reflection coefficients, and the angles Ψ and Δ are the raw data collected in a measurement as functions of λ. All our films can be considered as completely opaque, and can be described by the reflection coefficients

$$r_p = \frac{\langle\varepsilon\rangle\cos\vartheta - \sqrt{\langle\varepsilon\rangle - \sin^2\vartheta}}{\langle\varepsilon\rangle\cos\vartheta + \sqrt{\langle\varepsilon\rangle - \sin^2\vartheta}}, \quad r_s = \frac{\cos\vartheta - \sqrt{\langle\varepsilon\rangle - \sin^2\vartheta}}{\cos\vartheta + \sqrt{\langle\varepsilon\rangle - \sin^2\vartheta}}, \tag{3}$$

where ϑ is the angle of incidence and $\langle\varepsilon\rangle = \langle\varepsilon(\lambda)\rangle$ is the "pseudodielectric" function of the films. The term "pseudo" is used here since the films may not be completely isotropic or uniform; they are rough and may contain absorbed layers of different origins because they have been exposed to air. If this is the case then the dielectric function extracted from the raw data will be influenced by these factors. For our films we expect high level of isotropy but they may be not uniform in depth. It means that the dielectric function we extract from the data will be averaged over the distance of the order of the penetration depth. The roughness and absorbed layer can have some significance in the visible and ultraviolet ranges but not in the infrared, where the absorption on free electrons of metals is very large. Moreover, the effect of roughness is expected to be small since for all films w is much smaller than the smallest wavelength 137 nm. Because the infrared domain is the most important for the Casimir force we will consider $\langle\varepsilon(\lambda)\rangle$ extracted from the raw data as a good approximation for the dielectric function of the top layer of a gold film.

The dielectric function is connected with the ellipsometric parameter ρ for an isotropic and uniform solid as

$$\varepsilon = \sin^2\vartheta\left[1 + \tan^2\vartheta\left(\frac{1-\rho}{1+\rho}\right)^2\right]. \tag{4}$$

Instead of using ε a material is often characterized by the complex refractive index $\tilde{n} = n + ik = \sqrt{\varepsilon}$, where n is the refrac-
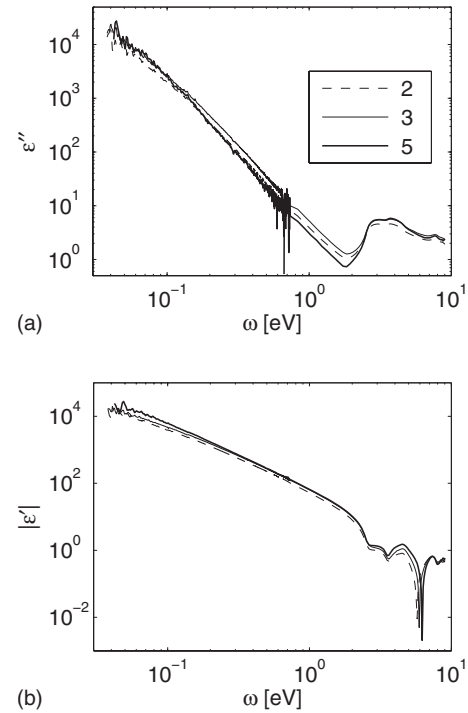

FIG. 2. (a) Measured ε'' as a function of frequency ω. (b) The same for $|\varepsilon'|$.

tive index and k is the extinction coefficient. Both descriptions are equivalent but the noise in the data is weighted differently, and it can influence to some degree the values of the Drude parameters (see next section).

Figure 2(a) shows the experimental results for $\varepsilon''(\omega)$ found via Eq. (4) for three different films. One can see that the IR-VASE gives a noisy signal at both ends of the spectral interval. The noise is significant for $\lambda > 20$ μm but the number of points in this range is not large, and the weight of these points for the extraction of the Drude parameters or Kramers-Kronig analysis is small. Around the interband transition (minimum of the the curves) the smallest absorption is observed for the annealed sample on mica indicating the smallest number of defects in the sample.[32] On the contrary, this sample shows the largest $|\varepsilon'|$ in the infrared as one can see in Fig. 1(b). An important conclusion that can be drawn from our measurements is the sample dependence of the dielectric function. The log-log scale is not very convenient for having an impression of this dependence. We present in Table I the values of ε for all five samples at chosen wavelengths $\lambda = 1, 5, 10$ μm. One can see that the real part of ε varies very significantly from sample to sample.

The sample dependence of the dielectric function can be partly attributed to different volumes of voids in the films as was proposed by Aspnes *et al.*[32] To check this assumption we did standard x-ray reflectivity (XRR) measurements[33–35] for the 100, 200, and 400 nm Au films on Si, which were deposited at identical conditions. From this kind of measurements one can draw information on the density of thin films. For this purpose the Phillips Xpert diffractometer on the Cu $K\alpha$ radiation line $\lambda = 1.54$ Å was used. The angle between the source and the surface was increased from 0.06° to 2°. For

TABLE I. Dielectric function for different samples at fixed wavelengths $\lambda = 1, 5, 10 \ \mu$m.

Sample	$\lambda = 1 \ \mu$m	$\lambda = 5 \ \mu$m	$\lambda = 10 \ \mu$m
1, 400 nm/Si	$-29.7 + i2.1$	$-805.9 + i185.4$	$-2605.1 + i1096.3$
2, 200 nm/Si	$-31.9 + i2.3$	$-855.9 + i195.8$	$-2778.6 + i1212.0$
3, 100 nm/Si	$-39.1 + i2.9$	$-1025.2 + i264.8$	$-3349.0 + i1574.8$
4, 120 nm/Si	$-43.8 + i2.6$	$-1166.9 + i213.9$	$-3957.2 + i1500.1$
5, 120 nm/mica	$-40.7 + i1.7$	$-1120.2 + i178.1$	$-4085.4 + i1440.3$

hard x rays the refractive index can be present as $n \approx 1 - \delta$, where $\delta \ll 1$ and we neglect the imaginary part of n since absorption is small. For gold δ is given

$$\delta = \frac{Z}{2\pi} N_a \frac{e^2}{4\pi\varepsilon_0 mc^2} \lambda^2 \approx 2.70 \times 10^{-6} \frac{N_e}{1 \ \text{cm}^{-3}} \left(\frac{\lambda}{1 \ \text{Å}} \right)^2,$$

(5)

where Z is the atomic number, N_a is the number of atoms per unit volume, ε_0 is the permittivity of vacuum, and $N_e = ZN_a$ is the density of electrons.

Since x rays refract away from the normal on the surface (refractive index $n < 1$), there exists a critical angle. Below this angle the total reflection occurs. The critical angle θ_c can be related to δ as $\theta_c \approx \sqrt{2\delta}$. Therefore, by measuring θ_c one can obtain knowledge of the electron density N_e. The XRR results are shown in Fig. 3. For very small angles the reflectivity decreases (not shown here), which may be due to the beam falling off the sample. Below the critical angle the material reflectivity is generally not very well understood, but it is of no concern to us since we are only interested in the region around θ_c. The transition region is clearly visible on the graph. Above the critical angle the signal drops very fast. The slope depends on the surface roughness. It is clear from the graph that the 100 nm film (sample 3) has the largest critical angle and, therefore, the largest electron density N_e. For bulk gold we have $N_e \approx 4.67 \times 10^{24} \ \text{cm}^{-3}$. For our films we found from the critical angles $N_e \approx (4.5 \pm 0.8) \times 10^{24} \ \text{cm}^{-3}$ for sample 3 and $N_e \approx (3.6 \pm 0.8) \times 10^{24} \ \text{cm}^{-3}$ for the two other films. The errors are rather large because $N_e \sim \theta_c^2$ and the curve is not sharp at θ_c. From this measure-
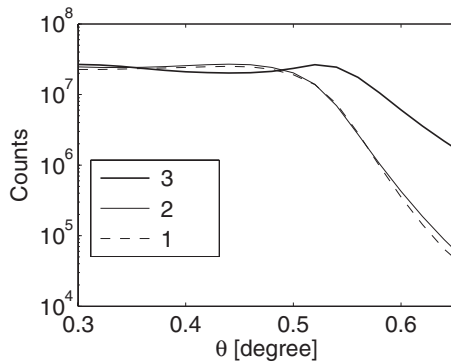

FIG. 3. X-ray reflectivity (counts) vs the angle of incidence (degrees). All three films were deposited at similar conditions.
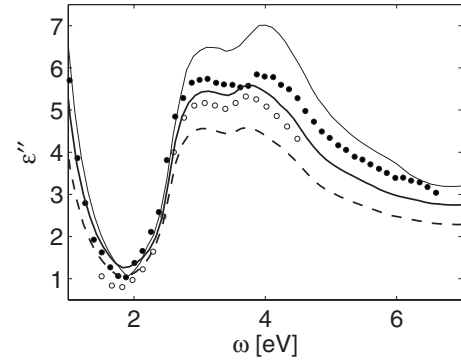

FIG. 4. Imaginary part of the dielectric function in the interband region obtained in different experiments. The thin solid line represents the data by Thèye (Ref. 36), the solid circles are the data by Johnson and Christy (Ref. 37), and the open circles are the data by Wang *et al.* (Ref. 38). The data of this study are presented by thick solid (sample 3) and thick dashed (sample 2) lines.

ment we cannot extract quantitative information, but qualitatively it agrees with the suggestion of different volumes of voids in the films.

A. Comparison with the existing data

In the interband absorption region ($\omega > 2.45$ eV) there is a significant amount of data obtained by combined reflectance and transmittance, ellipsometric spectroscopies on unannealed or annealed thin films, or bulk samples measured in air or ultrahigh vacuum. For comparison we have chosen the films by Thèye[36] evaporated in ultrahigh vacuum ($10^{-10} - 10^{-11}$ Torr) in the thickness range $10 - 25$ nm and being well annealed. These films represent the bulklike material. The data were collected by measuring reflectance and transmittance of the films. The Thèye data became part of the handbook table[18] in the range $1 < \omega < 6$ eV. The second choice is the data by Johnson and Christy.[37] These films $25 - 50$ nm thick and they were thermally evaporated in vacuum at 10^{-6} Torr. The data were collected for unannealed films from reflection and transmission measurements. As the third choice we took the data by Wang *et al.*[38] The films were thermally evaporated at pressure 10^{-5} Torr. The data were collected with spectroscopic ellipsometry for unannealed films of thickness 150 nm. The preparation conditions and the method of measurement are similar to that for our films.

The imaginary part of the dielectric functions, $\varepsilon''(\omega)$, for the chosen experiments are shown in Fig. 4 together with our data in the interband range. One can see that in this range of frequencies our data are rather typical. Only the Thèye films, obtained in ultrahigh vacuum and being well annealed, have significantly larger interband absorption. It should be mentioned that the interband absorption correlates with the film thickness: the thicker the film, the less it absorbs. The smallest absorption is observed for our 200 nm film. Wang *et al.*[38] deposited their films at the bottom of Dove prisms and measured the optical response on gold-air and gold-glass interfaces. They have found that the interband absorption on the gold-glass interface is larger than that on the gold-air inter-
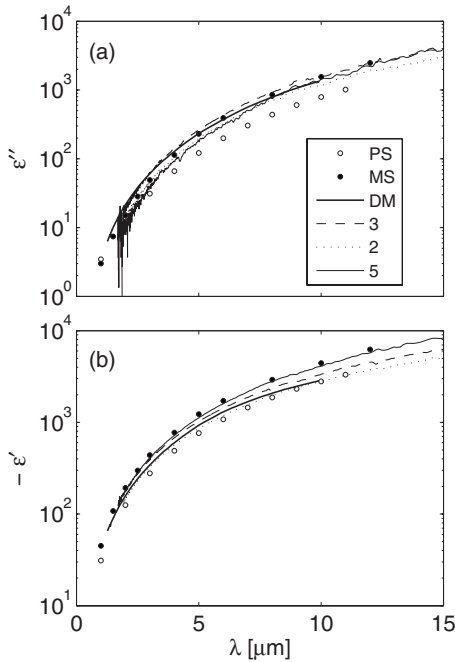
FIG. 5. Comparison of existing low-frequency data for gold. Panel (a) gives ε'' and panel (b) shows $-\varepsilon'$ as functions of the wavelength. The literature data are marked as PM (Ref. [41]), MS (Ref. [40]), and DM (Ref. [39]) [included in the handbook Ref. [18]]. Our data are presented for samples 2, 3, and 5.

face. In the former case the absorption is close to that observed by Thèye. It can be attributed to more dense packing of Au atoms nearby the substrate.

In the infrared and especially in mid- and far infrared the experimental data are sparse. In this range of frequencies both ε' and ε'' were measured only in a few studies.[39–41] Padalka and Shklarevskii[41] thermally evaporated the films on glass at pressure 10^{-5} Torr. The films were not annealed; the thickness of the films was not reported. They measured the optical constants in the range $1 < \lambda < 12$ μm. Motulevich and Shubin[40] evaporated gold on polished glass at pressure $\sim 10^{-6}$ torr. The investigated films were $0.5–1$ μm thick. The samples were annealed in the same vacuum at 400 °C. The optical constants n and k were measured by the polarization methods in the spectral range $1–12$ μm. Dold and Mecke did not describe the sample preparation carefully. It was only reported[39] that the films were evaporated onto a polished glass substrate, and measured in air by using an ellipsometric technique in the range $1.25–14$ μm. Presumably they were not annealed. These data are included in the handbook[18] table in the corresponding spectral range.

Figure 5 shows all the literature low-frequency data and three of our films. The main conclusion that can be drawn from this figure is that our films are typical in the sense of optical properties. This is because all the films were deposited at similar conditions. The annealed films by Motulevich and Shubin[40] and our annealed sample 5 show the largest $-\varepsilon'$.

III. ANALYSIS OF THE DATA

The Casimir force given by the Lifshitz formula depends on the dielectric function at imaginary frequencies: $\varepsilon(i\zeta)$.

This function cannot be measured directly in any experiment but with the help of the Kramers-Kronig relation it can be expressed via the observable function $\varepsilon''(\omega)$ as follows:

$$\varepsilon(i\zeta) = 1 + \frac{2}{\pi} \int_0^\infty d\omega \frac{\omega \varepsilon''(\omega)}{\omega^2 + \zeta^2}. \quad (6)$$

The experimental data available for $\varepsilon''(\omega)$ are always restricted from low and high frequencies. The low-frequency cutoff ω_{cut} is especially important in the case of metals. This is because for metals ε'' is large at low frequencies which contribute significantly to $\varepsilon(i\zeta)$.[23] Therefore, an important step in the evaluation of $\varepsilon(i\zeta)$ is extrapolation of the dielectric function $\varepsilon''(\omega)$ to low frequencies $\omega < \omega_{cut}$, where the experimental data are not accessible.

At low frequencies the dielectric function of metals can be described by the Drude function

$$\varepsilon(\omega) = 1 - \frac{\omega_p^2}{\omega(\omega + i\omega_\tau)}, \quad (7)$$

which is defined by two parameters, the plasma frequency ω_p and the relaxation frequency ω_τ. Lambrecht and Reynaud[42] fixed the plasma frequency using the relation

$$\omega_p^2 = \frac{Ne^2}{\varepsilon_0 m_e^*}, \quad (8)$$

where N is the number of conduction electrons per unit volume, e is the charge, and m_e^* is the effective mass of electron. The plasma frequency was evaluated assuming that each atom gives one conduction electron and that the effective mass coincides with the mass of free electron. The bulk density of Au was used to estimate N. The value of $\omega_p = 9.0$ eV found in this way was largely adopted by the community.[4–10] A relatively close value of ω_p was found by Bennett and Bennett[43] for carefully prepared films deposited in ultrahigh vacuum.[44] However, it was stressed by these authors that the reflectance for their films was always higher than the values reported for films under standard vacuum conditions. The value $\omega_p = 9.0$ eV is close to the plasma frequency in a perfect single crystal but the films used for measurement of the Casimir force can contain defects, which are responsible for the reduction of ω_p. The most important defects are small voids, which were observed in gold films with transmission electron microscopy.[45,46]

Special investigation of the influence of the defects was undertaken by Aspnes *et al.*,[32] where it was stressed that films grown at different conditions have considerably different ε'' above the interband transition. The spectra qualitatively differ only by scaling factors as one can see in Fig. 4. The scaling behavior of the spectra was attributed to different volumes of voids in the films prepared by different methods.[32] Different kinds of defects will also contribute to the scattering of free electrons changing the relaxation frequency ω_τ. Many researches stressed that the conduction electrons are much more sensitive to slight changes in the material structure.[32,36,44,47] It is well known, for example, that the resistivity of a film can be significantly larger than the resistivity of the bulk material. At any rate, so far we

TABLE II. The Drude parameters determined by different methods described in the text. In all cases the statistical errors in the parameters are on the same level: $0.01-0.03$ meV for ω_p and $0.2-0.5$ meV for ω_τ. The last column shows the values of the parameters averaged on different methods and the corresponding rms errors.

Sample	Parameter	Joint ε', ε''	Joint n, k	KK ε'	KK n	Average
1	ω_p [eV]	6.70	6.87	6.88	6.83	6.82 ± 0.08
400 nm/Si	ω_τ [meV]	38.4	43.3	40.2	39.9	40.5 ± 2.1
2	ω_p	6.78	7.04	6.69	6.80	6.83 ± 0.15
200 nm/Si	ω_τ	40.7	45.3	36.1	36.0	39.5 ± 4.4
3	ω_p	7.79	7.94	7.80	7.84	7.84 ± 0.07
100 nm/Si	ω_τ	48.8	52.0	47.9	47.4	49.0 ± 2.1
4	ω_p	7.90	8.24	7.95	7.90	8.00 ± 0.16
120 nm/Si	ω_τ	37.1	41.4	35.2	29.2	35.7 ± 5.1
5	ω_p	8.37	8.41	8.27	8.46	8.38 ± 0.08
120 nm/mica	ω_τ	37.1	37.7	34.5	39.1	37.1 ± 1.9

have to conclude that both Drude parameters must be extracted from the optical data of the films, which are used for the Casimir force measurement. Below we describe a few ways to extract these parameters from our data.

A. Joint fit of ε' and ε''

Separating the real and imaginary parts of the Drude function (7) one finds for ε' and ε''

$$\varepsilon'(\omega) = 1 - \frac{\omega_p^2}{\omega^2 + \omega_\tau^2}, \quad \varepsilon''(\omega) = \frac{\omega_p^2 \omega_\tau}{\omega(\omega^2 + \omega_\tau^2)}. \quad (9)$$

These equations have to be true below the interband transition $\hbar\omega < 2.45$ eV ($\lambda > 0.5$ μm),[36] but because this transition is not sharp one has to do analysis at lower frequencies. Practically Eq. (9) can be applied at wavelengths $\lambda > 2$ μm that coincides with the range of the infrared ellipsometer. In this range Eq. (9) can be compared with the optical data for both $\varepsilon'(\omega)$ and $\varepsilon''(\omega)$. Minimizing deviations between the data and theoretical expectations one can find the Drude parameters ω_p and ω_τ. For example, for sample 3 (100 nm, Au/Si) we found $\omega_p = 7.79 \pm 0.01$ eV and $\omega_\tau = 48.8 \pm 0.2$ meV. Similar calculations for annealed sample 5 (120 nm, Au/mica) gave $\omega_p = 8.37 \pm 0.03$ eV and $\omega_\tau = 37.1 \pm 0.5$ meV. The statistical uncertainty of the Drude parameters was found using a χ^2 criterion for joint estimation of two parameters.[48] For a given parameter the error corresponds to the change $\Delta\chi^2 = 1$ when the other parameter is kept constant. For all samples the values of the parameters are collected in Table II.

We found the parameters also in a slightly different way. One can fit the complex refractive index $\tilde{n}(\omega) = \sqrt{\varepsilon(\omega)}$ instead of the dielectric function. In the Drude range, where nearly all absorption is due to free electrons in the metal, $n(\omega)$ and $k(\omega)$ behave as

$$n(\omega) = \frac{\omega_p}{\sqrt{2}\omega_\tau} \frac{1}{\sqrt{1+y^2}} \left[1 + \frac{\sqrt{1+y^2}}{y}\right]^{-1/2}, \quad (10)$$

$$k(\omega) = \frac{\omega_p}{\sqrt{2}\omega_\tau} \frac{1}{\sqrt{1+y^2}} \left[1 + \frac{\sqrt{1+y^2}}{y}\right]^{1/2},$$

where $y = \omega/\omega_\tau$. Then we can minimize deviations for $n(\omega)$ and $k(\omega)$. The corresponding parameters for sample 3 are $\omega_p = 7.94 \pm 0.01$ eV and $\omega_\tau = 52.0 \pm 0.2$ meV. For the annealed sample 5 they are $\omega_p = 8.41 \pm 0.02$ eV and $\omega_\tau = 37.7 \pm 0.4$ meV. It can be noted that within the statistical errors the parameters for the annealed film are the same as those found by joint fit of ε' and ε''. However, for sample 3 this is not the case.

The Drude parameters should be the same in both cases but some difference can appear due to the smaller contributing weight of low frequencies when we perform minimization for n and k than that from the minimization of ε' and ε''. Figure 6 shows the data for $\varepsilon'(\lambda)$ and $\varepsilon''(\lambda)$ (solid lines) and the best Drude fit (dashed lines) found by minimization of deviations for ε' and ε''. Panel (a) corresponds to sample 5 and panel (b) shows the data for sample 3. The film on mica is described well by the Drude dielectric function, but the film on Si demonstrates some deviations from the Drude behavior at $\lambda < 15$ μm. It looks like an additional absorption band. In principle, the anomalous skin effect can be responsible for absorption in this range, but we found that this effect can be observable only at smaller ω_τ. Additional absorption in the Drude range is often observed due to the tail of the interband transition, but this is hardly the case because the wavelength is too large.

In absence of information on the origin of this absorption band we did phenomenological analysis of our data with the dielectric function, which includes an additional Lorentz oscillator

$$\varepsilon(\omega) = \varepsilon_D(\omega) + \frac{S\omega_0^2}{\omega_0^2 - \omega^2 - i\gamma\omega}, \quad (11)$$

where ε_D is the Drude function (7), S is the dimensionless oscillator strength, and ω_0 and γ are the central frequency
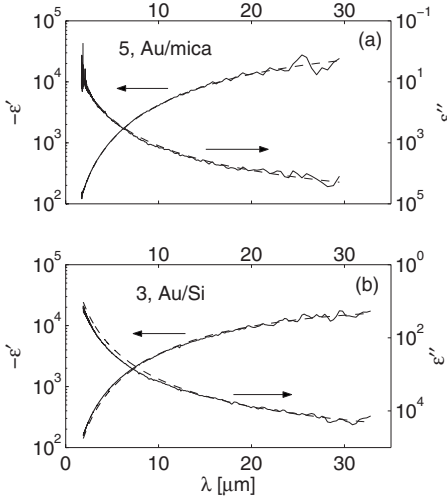
FIG. 6. The infrared data as functions of the wavelength λ for ε' and ε'' (solid lines) and the best Drude fits (dashed lines) for two gold films. Panel (a) shows the data for annealed sample 5 and panel (b) shows the same for unannealed sample 3.

and width of the band, respectively. Figure 7 shows the difference $\Delta\varepsilon'' = \varepsilon'' - \varepsilon''_D$ as a function of the wavelength λ. The smallest absorption is realized for the annealed film on mica. It becomes larger for the unannealed 100 nm film on Si, and increases further for the 200 nm film on Si. On the other hand, the central wavelength of the band and its width do not change significantly from sample to sample showing the common origin of the band for different samples. This situation can be expected if the samples differ only by the density of defects of the same kind. However, without additional experimental information we cannot specify the exact nature of these defects.

B. Determination of the parameters using the Kramers-Kronig relation

One of the disadvantages of the ellipsometric determination of the dielectric function is that the method does not maintain Kramers-Kronig (KK) consistency. Therefore, it is important to check the KK relations for our data. To do the KK analysis we also have to extrapolate the dielectric func-
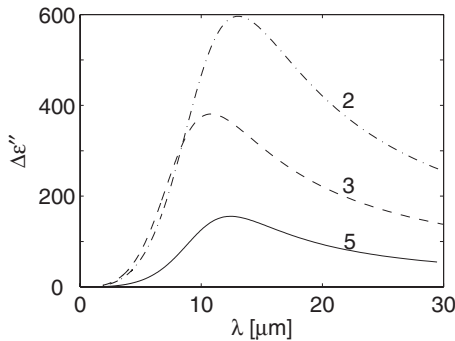

FIG. 7. Additional absorption band for samples 2, 3, and 5 as a function of the wavelength.

tion outside of the measured frequency range. For metals extrapolation to low frequencies is based again on the Drude dielectric function (7). It means that together with KK consistency we will find the Drude parameters for which this consistency is the best. This method for determining the Drude parameters was used recently[24] for analysis of the optical properties of gold samples, which are available in the literature.

The KK relation expresses $\varepsilon'(\omega)$ as integral over all frequencies of $\varepsilon''(\omega)$ as follows:

$$\varepsilon'(\omega) - 1 = \frac{2}{\pi} P \int_0^\infty dx \frac{x\varepsilon''(x)}{x^2 - \omega^2}, \tag{12}$$

where P means the principal part of the integral. To use this relation we have to define $\varepsilon''(\omega)$ at all frequencies. Below the low-frequency cutoff we define it using Eq. (9). Above the high-frequency cutoff (9 eV for our data) we enlarge the frequency range by using the handbook data[18] in the range $9 < \omega < 100$ eV and above 100 eV $\varepsilon''(\omega)$ is extrapolated as A/ω^3. The constant A is determined by matching ε'' at $\omega = 100$ eV. The principal part of the integral in Eq. (12) is calculated in the same way as in Ref. 24. $\varepsilon'(\omega)$ was calculated in the frequency range $0.01 < \omega < 100$ eV as a function of the Drude parameters. This function was compared with the measured one and minimization of deviations gave us the values of the parameters. The points outside of the measured frequency range ($\omega < 0.038$ eV) were compared with the prediction based on Eq. (9).

For sample 3 it was found $\omega_p = 7.80$ eV and $\omega_\tau = 47.9$ meV. The experimental function $\varepsilon'(\omega)$ continued to lower frequency according to the Drude model and its prediction based on the relation (12) is shown in Fig. 8 by thick and thin lines, respectively. The agreement between the curves is rather good. At high frequencies where $|\varepsilon'| \sim 1$ the logarithmic scale is not convenient for comparison. Instead we present in the inset the region bounded by the dotted rectangular in the linear scale. In this range the positions of the peaks are reproduced very well, but their magnitude is slightly different. This is because we used the data for ε'' above 9 eV from the handbook, which did not match precisely to those for our sample. Similar situation is realized for all the other films. The Drude parameters for all samples are presented in Table II.

Alternatively one can use the experimental extinction coefficient $k(\omega)$ to get the refractive index $n(\omega)$ using the KK relation between n and k as follows:

$$n(\omega) - 1 = \frac{2}{\pi} P \int_0^\infty dx \frac{xk(x)}{x^2 - \omega^2}. \tag{13}$$

At frequencies for which the experimental data are not accessible we define $k(\omega) = \text{Im} \sqrt{\varepsilon(\omega)}$, where $\varepsilon(\omega)$ continued to low frequencies according to Eq. (7) and to high frequencies as $\varepsilon(\omega) = 1 - \omega_p^2/\omega^2 + iA/\omega^3$. The constant A again is chosen by matching ε'' at the highest-frequency $\omega = 100$ eV.

In contrast with the KK relation (12) now we cannot present the contribution of low frequencies to the dispersion
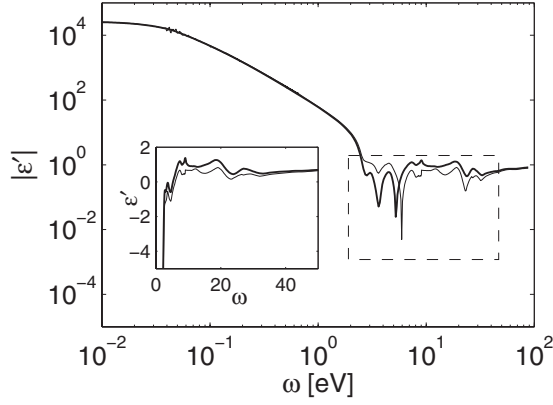
FIG. 8. Dielectric function ε' as a function of ω for sample 3. The thick line is the experimental curve extrapolated to the frequencies lower than 0.038 eV according to the Drude model. The thin line is the same function calculated from the KK relation (12). The Inset shows the behavior of ε' inside of the dotted rectangular in the linear scale.

FIG. 9. Refractive index n as a function of ω for sample 3. The thick line is the experimental curve extrapolated to $\omega < 0.038$ eV according to the Drude model. The thin line is the same function calculated from the KK relation (13). The inset shows the behavior of n in the linear scale in the range $0.5 < \omega < 50$ eV.

integral (13) in the analytic form. The Drude representation (10) for $k(\omega)$ at $\omega \ll \omega_p$ is

$$k(\omega) = \frac{\omega_p}{\sqrt{2}\omega_\tau}\left[\frac{1}{y\sqrt{1+y^2}} + \frac{1}{1+y^2}\right]^{1/2}, \quad (14)$$

where $y = \omega/\omega_\tau$. This function of y was approximated by the fourth order polynomial in y in the range $0 < y < 2$. With this polynomial the contribution of low frequencies to Eq. (13) was found analytically. Minimization of deviations between the experimental values of $n(\omega)$ and the theoretical predictions via Eq. (13) gave the values of the Drude parameters.

For sample 3 it was found $\omega_p = 7.84$ eV and $\omega_\tau = 47.4$ meV. The experimental and predicted curves for $n(\omega)$ are shown in Fig. 9 by thick and thin lines, respectively. The inset shows the same functions in the linear plot in the range $0.5 < \omega < 50$ eV. Again we have a reasonable agreement of the experiment and prediction on the basis of the KK relation.

The values of the Drude parameters found by different methods described above are collected in Table II. The statistical errors in the parameters are rather small. They do not depend significantly on the method and vary only slightly from sample to sample. These errors are 0.01–0.03 eV for ω_p and 0.2–0.5 meV for ω_τ. As one can see from Table II the values found by different methods do not agree with each other within the statistical errors. This is because each method treats noise in the data differently. We cannot give preference to any specific method. Instead, we average the values of the parameters determined by different methods, and define the root-mean-square (rms) error of this averaging as uncertainty in the parameter value. The averaged parameters and rms errors are given in the last column of Table II. Samples 1 and 2 have similar Drude parameters, which cannot be resolved within the discussed uncertainty, but all the other samples are clearly different.
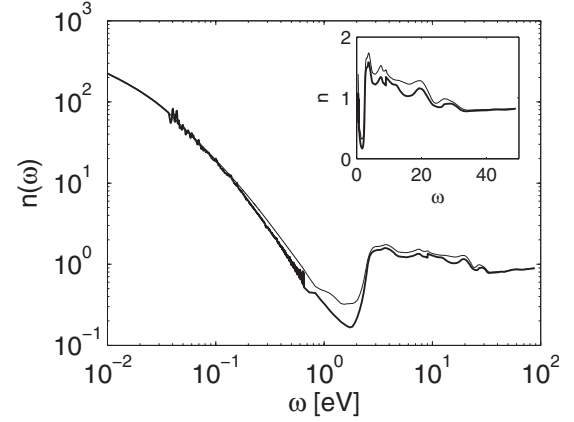
IV. SENSITIVITY OF THE CASIMIR FORCE TO THE OPTICAL PROPERTIES OF GOLD FILMS

In this section we are going to discuss the Casimir force without temperature or roughness corrections in order to concentrate on the influence of the material optical properties on the force. In this case the force between two similar parallel plates can be calculated using the Lifshitz formula[13]

$$F_{pp}(a) = -\frac{\hbar}{2\pi^2}\int_0^\infty d\zeta \int_0^\infty dq q k_0 \sum_{\mu=s,p} \frac{r_\mu^2 e^{-2ak_0}}{1 - r_\mu^2 e^{-2ak_0}}, \quad (15)$$

where $\mathbf{q}$ is the wave vector along the plates ($q = |\mathbf{q}|$). The formula includes the reflection coefficients for two polarization states $\mu = s$ and $\mu = p$ which are defined as

$$r_s = \frac{k_0 - k_1}{k_0 + k_1}, \quad r_p = \frac{\varepsilon(i\zeta)k_0 - k_1}{\varepsilon(i\zeta)k_0 + k_1} \quad (16)$$

with k_0 and k_1 being the normal components of the wave vector in vacuum and metal, respectively,

$$k_0 = \sqrt{\zeta^2/c^2 + q^2}, \quad k_1 = \sqrt{\varepsilon(i\zeta)\zeta^2/c^2 + q^2}. \quad (17)$$

A. Dielectric function at imaginary frequencies

To evaluate the force with the Lifshitz formula one has to know the dielectric function of the material at imaginary frequencies $\varepsilon(i\zeta)$, which is calculated via $\varepsilon''(\omega)$ according to Eq. (6). Therefore, first we have to calculate $\varepsilon(i\zeta)$ using our optical data. For this purpose let us present $\varepsilon(i\zeta)$ as

$$\varepsilon(i\zeta) = 1 + \varepsilon_{cut}(i\zeta) + \varepsilon_{expt}(i\zeta), \quad (18)$$

where ε_{cut} is calculated with the extrapolated $\varepsilon''(\omega)$ in the unaccessible frequency range $\omega < \omega_{cut}$, while ε_{expt} is calculated using the experimental data for $\varepsilon''(\omega)$, according to the formulas:
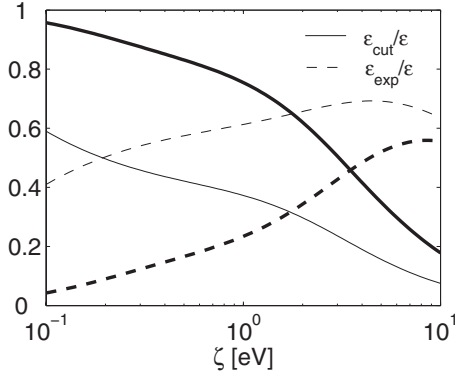
FIG. 10. Relative contribution of low ($\omega < \omega_{cut}$) and high ($\omega > \omega_{cut}$) frequencies to the dielectric function $\varepsilon(i\zeta)$ for our sample 3 (thin lines) and for the handbook data (Ref. 18) (thick lines).

$$\varepsilon_{cut}(i\zeta) = \frac{2}{\pi} \int_0^{\omega_{cut}} d\omega \frac{\omega \varepsilon''(\omega)}{\zeta^2 + \omega^2}, \quad \varepsilon_{expt}(i\zeta) = \frac{2}{\pi} \int_{\omega_{cut}}^{\infty} d\omega \frac{\omega \varepsilon''(\omega)}{\zeta^2 + \omega^2}.$$

(19)

Strictly speaking, we included in ε_{expt} the extrapolation to high frequencies, $\omega > 100$ eV, but this is justified because these frequencies do not play a very significant role. The high-frequency extrapolation of $\varepsilon''(\omega)$ was done in the same way as in Sec. III B so as the calculation of the integral for ε_{expt}. For the low-frequency extrapolation the Drude model (9) was used. In this case the integral for ε_{cut} can be found analytically, and it yields

$$\varepsilon_{cut}(i\zeta) = \frac{2}{\pi} \frac{\omega_p^2}{\zeta^2 - \omega_\tau^2} \left[\tan^{-1}\left(\frac{\omega_{cut}}{\omega_\tau}\right) - \frac{\omega_\tau}{\zeta} \tan^{-1}\left(\frac{\omega_{cut}}{\zeta}\right) \right].$$

(20)

Note that there is no singularity here at $\zeta = \omega_\tau$.

It was already stressed that for metals ε_{cut} gives an important contribution to the dielectric function. Of course, it depends on the value of ω_{cut}. For all previous data this value was around 0.125 eV. In this study $\omega_{cut} = 0.038$ eV is about three times smaller, but still the contribution of ε_{cut} is significant. It can be seen from Fig. 10, where the relative values $\varepsilon_{cut}(i\zeta)/\varepsilon(i\zeta)$ and $\varepsilon_{expt}(i\zeta)/\varepsilon(i\zeta)$ are presented for sample 3 as thin lines. For comparison in the same plot we showed (thick lines) ε_{cut} and ε_{expt} calculated with the handbook data, and extrapolated to $\omega < 0.125$ eV with the Drude parameters $\omega_p = 9.0$ eV and $\omega_\tau = 35$ meV. It should be stressed that for our film the contribution from the extrapolated region, ε_{cut}, dominates at $\zeta < 0.2$ eV, while for the handbook data it dominates up to $\zeta = 4$ eV. This is the result of reduced ω_{cut} for our data. It means that the calculations based on our data are more reliable because a smaller part of $\varepsilon(i\zeta)$ depends on the extrapolation.

The total dielectric functions $\varepsilon_i(i\zeta)$ (i is the number of the sample) are presented in Fig. 11(a) for samples 2, 3, and 5. The results for samples 1 and 4 are not shown for clarity. The thick solid line represents $\varepsilon_0(i\zeta)$, which is typically used for the Casimir force calculation. In this case the integral for ε_{expt} is evaluated for $\varepsilon''(\omega)$ taken from the handbook,[18] where
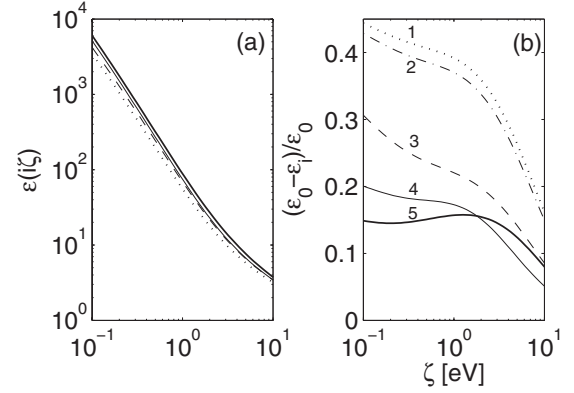

FIG. 11. (a) The dielectric function as a function of the imaginary frequency ζ. The thin dotted, dashed, and solid lines correspond to samples 2, 3, and 5, respectively. The thick line gives $\varepsilon_0(i\zeta)$ that is typically used for the Casimir force calculations. (b) Relative deviation of the dielectric function of the ith sample, ε_i, from ε_0.

the cutoff frequency is $\omega_{cut} = 0.125$ eV. The contribution of low frequencies, ε_{cut}, is calculated with the Drude parameters $\omega_p = 9.0$ eV and $\omega_\tau = 35$ meV.[42] In what follows we are using $\varepsilon_0(i\zeta)$ as a reference case.

Important contribution to the Casimir force comes from the imaginary frequencies around the characteristic frequency $\zeta_{ch} = c/2a$. This frequency is in the range $0.1 \lesssim \zeta_{ch} \lesssim 10$ eV when the distance is in the most interesting interval 10 nm $\lesssim a \lesssim 1$ μm. The frequency range in Figs. 11(a) and 11(b) was chosen accordingly. The logarithmic scale in Fig. 11(a) does not give the feeling of actual difference between the curves. The relative change in the dielectric function $[\varepsilon_0(i\zeta) - \varepsilon_i(i\zeta)]/\varepsilon_0(i\zeta)$ demonstrates much better the significance of actual optical properties of the films. This change is shown in Fig. 11(b) for all our films. The deviation of $\varepsilon_i(i\zeta)$ from the imaginary material with the dielectric function $\varepsilon_0(i\zeta)$, which is described by the bulk Drude parameters and the handbook optical data, is significant at all important frequencies and for all samples. Of course, this deviation will be translated into the change in the Casimir force. The curves in Fig. 11(b) were calculated for the middle values of the Drude parameters in the last column of Table II. The uncertainty of these parameters is responsible for uncertainty of $\varepsilon_i(i\zeta)$. It is especially large for samples 2 and 4. We will discuss it later in connection with the uncertainty of the force.

B. Casimir force

To calculate the Casimir force the dielectric functions for all samples, $\varepsilon_i(i\zeta)$, were found numerically in the frequency range 0.01 eV $< \zeta < 100$ eV. At lower frequencies, $\zeta < 0.01$ eV, they were extrapolated according to the Drude model. At higher frequencies, $\zeta > 100$ eV, we extrapolated with the function $\varepsilon_i(i\zeta) = 1 + A_i/\zeta^2$, where for each sample the constant A_i was chosen to match the value of $\varepsilon_i(i\zeta)$ at $\zeta = 100$ eV.
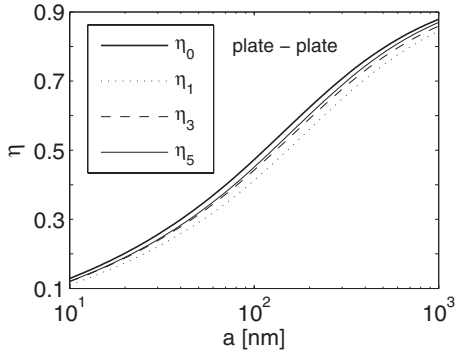
FIG. 12. Reduction factor η as a function of the separation a for samples 1, 3, and 5. The thick line shows the reference result calculated with $\varepsilon_0(i\zeta)$.
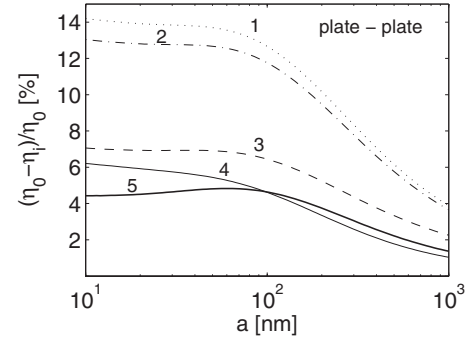

FIG. 13. Relative deviation of the reduction factors for different samples from the reference curve $\eta_0(a)$, which were evaluated using the handbook optical data (Ref. [18]) and the Drude parameters $\omega_p=9$ eV and $\omega_\tau=0.035$ eV.

It is convenient to calculate not the force itself but so called the reduction factor η_{pp}, which is defined as the ratio of the force to the Casimir force between ideal metals as follows:

$$\eta_{pp}(a) = \frac{F_{pp}(a)}{F_{pp}^c(a)}, \quad F_{pp}^c(a) = -\frac{\pi^2\hbar c}{240a^4}. \quad (21)$$

For convenience of the numerical procedure one can make an appropriate change of variables in Eq. (15) so that the reduction factor can be presented in the form

$$\eta_{pp}(a) = \frac{15}{2\pi^4} \sum_{\mu=s,p} \int_0^1 dx \int_0^\infty \frac{dy\, y^3}{r_\mu^{-2}e^y - 1}, \quad (22)$$

where the reflection coefficients as functions of x and y are defined as

$$r_s = \frac{1-s}{1+s}, \quad r_p = \frac{\varepsilon(i\zeta_{ch}xy) - s}{\varepsilon(i\zeta_{ch}xy) + s}, \quad (23)$$

with

$$s = \sqrt{1 + x^2[\varepsilon(i\zeta_{ch}xy) - 1]}, \quad \zeta_{ch} = \frac{c}{2a}. \quad (24)$$

The integral (22) was calculated numerically with different dielectric functions $\varepsilon_i(i\zeta)$ with a precision of 10^{-6}. The results are presented in Fig. 12 for samples 1, 3, and 5. The reference curve (thick line) calculated with $\varepsilon_0(i\zeta)$ is also shown for comparison. It represents the reduction factor, which is typically used in the precise calculations of the Casimir force between gold surfaces. One can see that there is a significant difference between this reference curve and those that correspond to actual gold films. To see the magnitude of the deviations from the reference curve, we plot in Fig. 13 the ratio $(\eta_0 - \eta_i)/\eta_0$ as a function of distance a for all five samples.

At small distances the deviations are more sensitive to the value of ω_p. At large distances the sample dependence becomes weaker and more sensitive to the value of ω_τ. For samples 1 and 2, which correspond to the 400 and 200 nm films deposited on the Si substrate, the deviations are especially large. They are 12%–14% at $a < 100$ nm and stay con-

siderably even for the distances as large as 1 μm. Samples 3, 4, and 5 have smaller deviations from the reference case but even for these samples the deviations are as large as 5%–7%.

We calculated also how uncertainty in the Drude parameters influences the uncertainty in the force. For this purpose we calculated the reduction factor η at the borders of the error intervals: $[\omega_p+\Delta\omega_p, \omega_\tau]$ and $[\omega_p, \omega_\tau-\Delta\omega_\tau]$, where $\Delta\omega_p$ and $\Delta\omega_\tau$ are shown as the errors in the last column of Table II. The results were compared with η calculated with the middle values of the parameters $[\omega_p, \omega_\tau]$. The maximal deviations were found for sample 4. The relative deviations for this sample, $\Delta\eta/\eta$, are shown in Fig. 14 as functions of the separation a. These deviations, $\Delta\eta/\eta$, are defined as

$$\frac{\Delta\eta}{\eta} = \frac{\eta(\omega_p,\omega_\tau,a) - \eta(\omega_p+\delta\omega_p,\omega_\tau+\delta\omega_\tau,a)}{\eta(\omega_p,\omega_\tau,a)}, \quad (25)$$

where the variations of the plasma and relaxation frequencies, $\delta\omega_p$ and $\delta\omega_\tau$, give the maximal effect on the reduction factor when $\delta\omega_p=\Delta\omega_p$ and $\delta\omega_\tau=-\Delta\omega_\tau$.

In most of the experiments the force was measured between a gold covered sphere and a plate. In the case of the sphere-plate interaction we define the reduction factor as
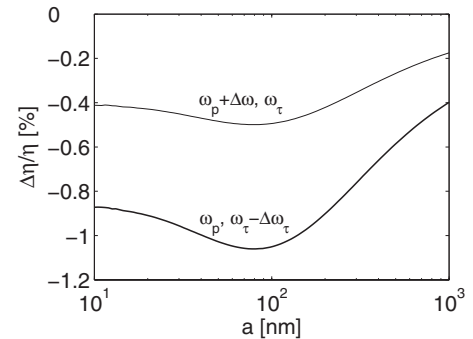

FIG. 14. Relative variation of the reduction factor (see definition in the text) for the Drude parameters at the sides of the error intervals. The results are presented for sample 4.

$$\eta_{sp}(a) = \frac{F_{sp}(a)}{F_{sp}^c(a)}, \quad F_{sp}^c(a) = -\frac{\pi^3 R\hbar c}{360a^3}, \quad (26)$$

where R is the sphere radius. The expression convenient for numerical calculations in this case is the following:

$$\eta_{sp}(a) = -\frac{45}{2\pi^4}\sum_{\mu=s,p}\int_0^1 dx \int_0^\infty dy y^2 \ln(1 - r_\mu^2 e^{-y}), \quad (27)$$

where the reflection coefficients are defined in Eq. (23). Although in the case of sphere and plate the reduction factors are different from those between two plates, the qualitative behavior with the separation is the same. The relative deviations $(\eta_0 - \eta_i)/\eta_0$ for the sphere and plate are very close to those shown in Fig. 13, and we do not show this additional plot.

V. CONCLUSIONS

In this paper we analyzed the optical properties of gold films deposited with different techniques on silicon or mica substrates. The optical responses were measured ellipsometrically in a wide range of wavelengths. In the mid infrared our data cover the range of wavelengths up to 33 μm, which is larger than in all previous studies (~ 10 μm), where both the real and imaginary parts of the dielectric function were measured. The data unambiguously demonstrate the sample dependence of the dielectric function. It was found that thicker films are inferior in the optical sense than thin (but opaque) films. It is probably connected with more dense parking of atoms nearby the substrate. The x-ray reflectivity measurements qualitatively support this interpretation. We also observed some difference between samples deposited in the electron-beam evaporator or in the thermal evaporator, but it is possible that this difference is connected with different sublayers (titanium or chromium, respectively) on Si substrates.

The Casimir force depends on the dielectric function at imaginary frequencies, $\varepsilon(i\zeta)$, which is expressed via the measurable function $\varepsilon''(\omega)$ by the dispersion relation (6). For metals low frequencies play a very important role in this relation. However, in experiments there is a low-frequency cutoff, ω_{cut}, so that the data at smaller frequencies are not accessible. For a precise evaluation of the force, one has to extrapolate the measured $\varepsilon''(\omega)$ to the frequencies $\omega < \omega_{cut}$. For noble metals such as gold it can be done with the help of the Drude model. The parameters of the Drude model ω_p and

ω_τ have to be extracted from the optical data at $\omega > \omega_{cut}$. In this paper we found the Drude parameters for our films using joint fit of $\varepsilon'(\omega)$ and $\varepsilon''(\omega)$ and independently using the Kramers-Kronig consistency of the data. As an alternative we did the same analysis for the refraction index and the extinction coefficient. The results collected in Table II exhibit significant variation of the parameters from sample to sample. Moreover, the parameters are slightly different when different methods to fit the data are used. This is because the noise in the data are weighted differently for different methods of parameter determination. We defined the values and the errors in the parameters as the averaged values over different methods and the corresponding rms errors, respectively.

The contribution of the extrapolated part of $\varepsilon''(\omega)$ to $\varepsilon(i\zeta)$ is considerably smaller for our data than for the handbook data as one can see in Fig. 10. The reason is that in our case the cutoff frequency $\omega_{cut}=0.0378$ eV is smaller than that for the handbook data, where $\omega_{cut}=0.125$ eV. Nevertheless, this contribution is still significant and has to be carefully considered. As a reference curve for $\varepsilon(i\zeta)$ we have chosen $\varepsilon_0(i\zeta)$, which was calculated with the handbook data for $\omega > 0.125$ eV, and extrapolated for smaller frequencies with the Drude parameters $\omega_p=9.0$ eV and $\omega_\tau=35$ meV. This curve is typically used for the calculation of the Casimir force. For our films we have found that $\varepsilon_i(i\zeta)$ was always smaller than the reference curve, and the relative deviation is larger than 15% at $\zeta \sim 1$ eV [see Fig. 11(b)].

Indeed, the Casimir force evaluated for our films is considerably smaller from that calculated with the reference curve $\varepsilon_0(i\zeta)$. The smallest deviation is realized for sample 5 (120 nm Au/mica) and estimated to be 4%–5% in the distance range $a \lesssim 200$ nm. For thicker films (sample 1 or 2) it can be as large as 14% (see Fig. 13). At large separations the sample dependence becomes weaker, but it is above 1% even at $a=1$ μm.

Our main conclusion is that actual optical properties of the materials used for the measurement of the Casimir force are very important for comparison between theory and experiment. These properties have to be measured for the same materials, and not taken from a handbook for a material of the same chemical nature but possibly of very different microstructure. It is concluded that prediction of the Casimir force with a precision better than 10% must be based on the material optical response measured from visible to mid-infrared range.

*Author to whom correspondence should be addressed; v.b.svetovoy@ewi.utwente.nl

[1] H. B. G. Casimir, Proc. K. Ned. Akad. Wet. **51**, 793 (1948).
[2] S. K. Lamoreaux, Phys. Rev. Lett. **78**, 5 (1997); **81**, 5475 (1998).
[3] U. Mohideen and A. Roy, Phys. Rev. Lett. **81**, 4549 (1998); A. Roy, C.-Y. Lin, and U. Mohideen, Phys. Rev. D **60**, 111101(R) (1999).
[4] B. W. Harris, F. Chen, and U. Mohideen, Phys. Rev. A **62**,

052109 (2000).
[5] H. B. Chan, V. A. Aksyuk, R. N. Kleiman, D. J. Bishop, and F. Capasso, Science **291**, 1941 (2001); Phys. Rev. Lett. **87**, 211801 (2001).
[6] R. S. Decca, D. López, E. Fischbach, and D. E. Krause, Phys. Rev. Lett. **91**, 050402 (2003).
[7] R. S. Decca, E. Fischbach, G. L. Klimchitskaya, D. E. Krause, D. López, and V. M. Mostepanenko, Phys. Rev. D **68**, 116003

(2003).

[8] R. S. Decca, D. López, E. Fischbach, G. L. Klimchitskaya, D. E. Krause, and V. M. Mostepanenko, Ann. Phys. (N.Y.) **318**, 37 (2005).

[9] G. Bressi, G. Carugno, R. Onofrio, and G. Ruoso, Phys. Rev. Lett. **88**, 041804 (2002).

[10] T. Ederth, Phys. Rev. A **62**, 062104 (2000).

[11] E. M. Lifshitz, Zh. Eksp. Teor. Fiz. **29**, 94 (1956) [Sov. Phys. JETP **2**, 73 (1956)].

[12] I. E. Dzyaloshinskii, E. M. Lifshitz, and L. P. Pitaevskii, Adv. Phys. **38**, 165 (1961).

[13] E. M. Lifshitz and L. P. Pitaevskii, *Statistical Physics* (Pergamon, Oxford, 1980), pt. 2.

[14] G. L. Klimchitskaya and Yu. V. Pavlov, Int. J. Mod. Phys. A **11**, 3723 (1996).

[15] C. Genet, A. Lambrecht, P. Maia Neto, and S. Reynaud, Europhys. Lett. **62**, 484 (2003).

[16] Paulo A. Maia Neto, A. Lambrecht, and S. Reynaud, Phys. Rev. A **72**, 012115 (2005).

[17] G. L. Klimchitskaya, U. Mohideen, and V. M. Mostepanenko, Phys. Rev. A **61**, 062107 (2000).

[18] *Handbook of Optical Constants of Solids*, edited by E. D. Palik (Academic, New York, 1995).

[19] J. H. Weaver, C. Krafka, D. W. Lynch, and E. E. Koch, *Optical Properties of Metals, Part II, Physics Data No. 18-2* (Fachinformationszentrum Energie, Physik, Mathematik, Karsruhe, 1981).

[20] S. K. Lamoreaux, Phys. Rev. A **59**, R3149 (1999).

[21] S. K. Lamoreaux, Phys. Rev. Lett. **83**, 3340 (1999).

[22] V. B. Svetovoy and M. V. Lokhanin, Mod. Phys. Lett. A **15**, 1013 (2000).

[23] V. B. Svetovoy and M. V. Lokhanin, Mod. Phys. Lett. A **15**, 1437 (2000).

[24] I. Pirozhenko, A. Lambrecht, and V. B. Svetovoy, New J. Phys. **8**, 238 (2006).

[25] P. Meakin, Phys. Rep. **235**, 1991 (1994).

[26] J. Krim and G. Palasantzas, Int. J. Mod. Phys. B **9**, 599 (1995).

[27] Y.-P. Zhao, G.-C. Wang, and T.-M. Lu, *Characterization of Amorphous and Crystalline Rough Surfaces-Principles and Applications*, Experimental Methods in the Physical Science Vol. 37 (Academic, New York, 2001).

[28] P. van Zwol, G. Palasantzas, and J. Th. M. De Hosson, Appl. Phys. Lett. **91**, 144108 (2007).

[29] http://www.JAWoollam. com

[30] R. M. A. Azzam and N. M. Bashara, *Ellipsometry and Polarized Light* (North Holland, Amsterdam, 1987).

[31] H. G. Tompkins and W. A. McGahan, *Spectroscopic Ellipsometry and Reflectometry* (Wiley, New York, 1999).

[32] D. E. Aspnes, E. Kinsbron, and D. D. Bacon, Phys. Rev. B **21**, 3290 (1980).

[33] S. K. Sinha, E. B. Sirota, S. Garoff, and H. B. Stanley, Phys. Rev. B **38**, 2297 (1988).

[34] A. Braslau, P. S. Pershan, G. Swislow, B. M. Ocko, and J. Als-Nielsen, Phys. Rev. A **38**, 2457 (1988).

[35] J. Als-Nielsen, *Handbook of Synchrotron Radiation* (North-Holland, New York, 1991).

[36] M.-L. Thèye, Phys. Rev. B **2**, 3060 (1970).

[37] P. B. Johnson and R. W. Christy, Phys. Rev. B **6**, 4370 (1972).

[38] Yu Wang, Liang-Yao Chen, Bo Xu, Wei-Ming Zheng, Rong-Jun Zhang, Dong-Liang Qian, Shi-Ming Zhou, Yu-Xiang Zheng, Ning Dai, Yu-Mei Yang, Kou-Bao Ding, and Xiu-Miao Zhang, Thin Solid Films **313**, 232 (1998).

[39] B. Dold and R. Mecke, Optik (Stuttgart) **22**, 435 (1965).

[40] G. P. Motulevich and A. A. Shubin, Zh. Eksp. Teor. Fiz. **47**, 840 (1964) [Sov. Phys. JETP **20**, 560 (1965)].

[41] V. G. Padalka and I. N. Shklyarevskii, Opt. Spektrosk. **11**, 527 (1961) [Opt. Spectrosc. **11**, 285 (1961)].

[42] A. Lambrecht and S. Reynaud, Eur. Phys. J. D **8**, 309 (2000).

[43] H. E. Bennett and J. M. Bennett, in *Optical Properties and Electronic Structure of Metals and Alloys*, edited by F. Abélès (North-Holland, Amsterdam, 1966).

[44] J. M. Bennett and E. J. Ashley, Appl. Opt. **4**, 221 (1965).

[45] J. A. Lloyd and S. Nakahara, J. Appl. Phys. **48**, 5092 (1977).

[46] J. A. Lloyd and S. Nakahara, J. Vac. Sci. Technol. **14**, 655 (1977).

[47] N. Kaiser, Appl. Opt. **41**, 3053 (2002).

[48] K. Hagiwara, Hikasa, K. Nakamura, M. Tanabashi, M. Aguilar-Benitez, C. Amsler, R. M. Barnett, P. R. Burchat, C. D. Carone, C. Caso, G. Conforto, O. Dahl, M. Doser, S. Eidelman, J. L. Feng, L. Gibbons, M. Goodman, C. Grab, D. E. Groom, A. Gurtu, K. G. Hayes, J. J. Hernandez-Rey, K. Honscheid, C. Kolda, M. L. Mangano, D. M. Manley, A. V. Manohar, J. March-Russell, A. Masoni, R. Miguel, K. Mönig, H. Murayama, S. Navas, K. A. Olive, L. Pape, C. Patrignani, A. Piepke, M. Roos, J. Terning, N. A. Törnqvist, T. G. Trippe, P. Vogel, C. G. Wohl, R. L. Workman, and W.-M. Yao, Phys. Rev. D **66**, 010001 (2002).